molecules

MDPI

Article

Mechanism of One-Step Hydrothermally Synthesized Titanate Catalysts for Ozonation

Geshan Zhang [1,*], Anhua Jiang [2], Xinwen Huang [2,*], Tian Yuan [1], Hanrui Wu [1], Lichun Li [1] and Zongjian Liu [1]

[1] College of Chemical Engineering, Zhejiang University of Technology, Hangzhou 310014, China; 2111901017@zjut.edu.cn (T.Y.); 2112001011@zjut.edu.cn (H.W.); lichunli@zjut.edu.cn (L.L.); zjliu@zjut.edu.cn (Z.L.)

[2] College of Environment, Zhejiang University of Technology, Hangzhou 310014, China; 1111827011@zjut.edu.cn

* Correspondence: zhanggs@zjut.edu.cn (G.Z.); xwhuang@zjut.edu.cn (X.H.); Tel.: +86-571-8832-0412 (G.Z.)

Abstract: A titanate nanotube catalyst for ozonation was synthesized with a simple one-step NaOH hydrothermal treatment without energy-consuming calcination. The synthesized titania catalysts were characterized by X-ray diffraction (XRD), Raman, porosimetry analysis, high-resolution transmission electron microscopy (HR-TEM), Fourier transformed infrared (FTIR), and electron paramagnetic resonance (EPR) analysis. The catalyst treated with a higher concentration of NaOH was found to be more catalytically active for phenol removal due to its higher titanate content that would facilitate more OH groups on its surface. Furthermore, the main active oxidizing species of the catalytic ozonation process were recognized as singlet oxygen and superoxide radical, while the hydroxyl radical may only play a minor role. This work provides further support for the correlation between the properties of titania and catalytic performance, which is significant for understanding the mechanism of catalytic ozonation with titania-based materials.

Keywords: catalytic ozonation; titanate nanotube; active oxidizing species; phenol; water treatment

Citation: Zhang, G.; Jiang, A.; Huang, X.; Yuan, T.; Wu, H.; Li, L.; Liu, Z. Mechanism of One-Step Hydrothermally Synthesized Titanate Catalysts for Ozonation. *Molecules* **2022**, *27*, 2706. https://doi.org/10.3390/molecules27092706

Academic Editor: Alessandra Puglisi

Received: 28 March 2022
Accepted: 20 April 2022
Published: 22 April 2022

1. Introduction

Ozonation is one of the most widely applied technologies in drinking and waste water treatment plants for removing contaminants. However, it has unavoidable disadvantages, including a relatively high oxidizing selectivity and a high pH dependency, which limit its environmental application. For instance, the drinking water treatment plant revealed a cyano-HABs incident in 2013 in Lake Erie in Toledo (US) even with the ozone treatment [1]. Therefore, it is necessary to apply more advanced technologies to improve the effectiveness of the treatment [2–4].

A more economical approach is the modification of the existing ozonation process, i.e., catalytic ozonation [2,5,6]. This technology includes homogeneous catalytic ozonation and heterogeneous catalytic ozonation usually involving transition metals, while the latter would be more practical in water treatment plants due to its heterogeneity and relative immobility that would facilitate the subsequent treatment. Among these solid metals or metal oxide catalysts, many researchers believe TiO_2 is a type of effective catalyst that can enhance the oxidizing efficiency of the ozonation process. Dr. Song et al. stated that rutile TiO_2 with a higher specific surface area and more surface OH groups would have a higher catalytic activity for phenol removal [7]. Dr. Ma's research group synthesized several TiO_2 catalysts, including nano-TiO_2 [8], TiO_2/Silica-Gel [9] and TiO_2/Zeolite [10], which showed various catalytic behaviors for removing organic pollutants. Anandan et al. studied the degradation of fipronil with P25 TiO_2 catalytic ozonation treatment and achieved an improvement in efficiency of 15% compared to the ozone-only process [11]. The application of TiO_2 catalysts in ozonation would accelerate the generation of reactive radical species (such as hydroxyl radical, singlet oxygen, and superoxide radical) in the

system, which could result in a lower reaction selectivity and a higher reaction efficiency of ozonation for pollutant removal in water [1,9,12].

TiO_2 (or titanate) nanotubes have been studied for their chemical, synthetic and environmental application [13–15]. Kitano et al. synthesized a titanate nanotube derived from the scrolling of lamellar titanate nanosheets for benzyltoluene formation, which showed a higher catalytic activity due to its lattice distortion and mesoporous structure [16]. Titanate nanotubes have been studied for their adsorption and photocatalysis properties, showing that nanotubes with a lower Na content would have lower adsorption capacity but higher mineralization ability, while nanotubes calcined at 400–500 °C would promote photocatalytic activity [17,18]. In addition, titanate nanotubes were applied to improve the efficiency of ozonation. For instance, Liu et al. examined the effect of calcination temperature on the activity of TiO_2 catalytic ozonation and found lower annealing temperature would result in better catalytic activity for ammonia removal [19]; Xing et al. also found that titanate nanotubes could accelerate the degradation of *p*-nitrophenol in the ozonation process [20]. To the best of the authors' knowledge, all the applied titanate nanotubes were calcined before use, many of which were modified based on the reference [21]. In our preliminary experiment, titanate nanotubes without calcination were also found to be catalytically active, which is more efficient in energy utilization and hence attracted our research interest. Moreover, the correlation between the properties of nanotubes and the catalytic performance remains unclear, which is valuable for understanding the mechanism of catalytic ozonation with titania-based materials.

In this study, titania catalysts were synthesized using a simple hydrothermal process without calcination. The catalytic activities of these catalysts were evaluated for phenol (one of the most common and typical organic pollutants in various waters) removal during the ozonation process. The catalysts were characterized by several techniques and investigated for their essential properties responsible for their catalytic activity. Moreover, the main active oxidation species of catalytic ozonation were studied to unveil the catalytic mechanism.

2. Results and Discussion

2.1. Catalytic Activities of Titania Catalysts

The synthesized titania catalysts were tested for their catalytic activity during the ozonation of phenol. Figure 1 exhibits the concentration changes in phenol through ozonation catalyzed by TiO_2 (anatase or rutile) treated with different concentrations of NaOH in the hydrothermal process. Their corresponding pseudo-first-order rate constants of the degradation were calculated and compared (Figure S1 in Supplementary Material (SM)). As shown in Figure 1, the presence of raw rutile TiO_2 shows little impact on the ozonation rate of phenol, while raw anatase TiO_2 even has a suppressing effect on the ozonation. These results are consistent with many previous research works. Molnar et al. applied P25 TiO_2 in ozonation and found that a TiO_2 catalyst could not increase the efficiency of NOM removal in the ozonation process [22]. Dr. Ovelleiro's group examined P25 and synthesized TiO_2 for catalytic ozonation and concluded that these TiO_2 catalysts had no effect or even a negative effect on the ozonation [23,24]. Chen et al. prepared a TiO_2/Al_2O_3 catalyst and found the catalyst could not increase its removal efficiency but could enhance its TOC removal rate [25]. After the hydrothermal treatment with NaOH, the catalytic activities of TiO_2 materials can be significantly improved, while catalysts originating from rutile show slightly lower catalytic activity than those from anatase. Among these synthesized materials, anatase treated with 15 M NaOH (A-15) shows the highest catalytic activity with a rate constant of $0.0658 \pm 0.0114\ min^{-1}$, which is 4.2 times higher than that of raw anatase TiO_2. Compared to raw rutile TiO_2, the catalytic rate constant of R-15 ($0.0536 \pm 0.0045\ min^{-1}$) is 2 times higher. Moreover, the catalytic activity of the catalyst increases with the concentration of applied NaOH, indicating the key influence of NaOH in hydrothermal treatment during preparation. Compared to catalysts treated with 15 M NaOH (A-15 or R-15), catalysts treated with 10 M NaOH (A-10 or R-10) show slightly

lower activity: the catalytic rate constants of A-10 and R-10 are 0.0586 ± 0.0067 min^{-1} and 0.0511 ± 0.0026 min^{-1}, respectively. However, the washing process for catalysts treated with 15 M NaOH consumes much more acid reagent and needs more time in order to receive neutral catalysts, which is not environmentally friendly.

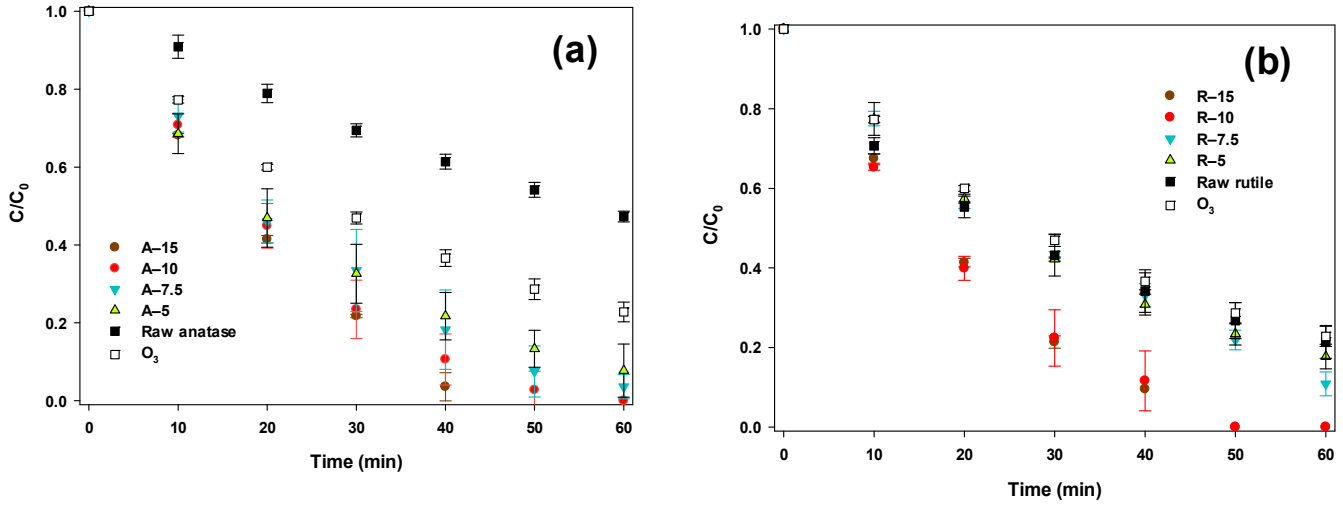

Figure 1. Catalytic activities of synthesized titania catalysts originating from anatase (**a**) or rutile (**b**). (Initial concentration of phenol is 20 mg/L; introduced O_3 is 10 mg/L with a flow rate of 50 mL/min).

The catalytic rates of titania catalysts treated with 10 M NaOH without calcination (samples 110-24) are also compared with those with calcination at 400 °C (samples 110-24-400), as shown in Figure 2. The catalytic efficiencies of samples originating from anatase with or without calcination show no significant difference in ozonation of phenol, while the catalyst originating from rutile without calcination shows a slightly higher rate. Song et al. attributed the catalytic activity of TiO_2 (including nanotubes with calcination) to its high specific surface area and its rutile crystallite phases in ozonation of phenol [7]. In addition, higher temperature or longer time of hydrothermal treatment (samples 180-24 and 110-48 in Figure 2) would depress the catalytic efficiency for ozonation of phenol, showing that the hydrothermal treatment at 110 °C for 24 h is appropriate. However, we still do not understand the mechanism of catalytic ozonation with titanate catalysts without calcination. Hence, further characterizations of these synthesized catalysts are needed in order to explore the correlation between the physico-chemical properties of the titanate materials and their catalytic performance in ozonation.

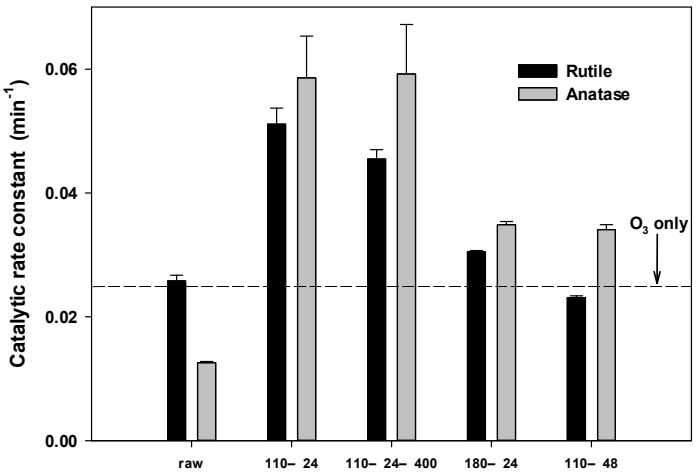

Figure 2. Catalytic rate constants of titania catalysts prepared under different synthesizing conditions.

2.2. Physico-Chemical Characteristics of Synthesized Titania Catalysts

The synthesized materials were firstly checked with HR-TEM for their morphology and crystallinity. As shown in Figure 3, a small number of titania nanotubes can be observed in sample A-5, while more nanotubes are displayed in the samples with a higher concentration of NaOH (i.e., 7.5 M and 10 M). In samples A-5 and A-7.5, the lattice spacings of anatase are measured to be 3.55 Å and 3.56 Å, respectively, which are very close to the value of raw anatase (3.54 Å). Almost all of the materials could be transformed into nanotubes when the samples were treated with 10 M NaOH, which are several hundred nanometers to several micrometers in length with a diameter of 5 to 40 nanometers (internal diameter of several nanometers). Regarding these samples (treated with NaOH ranging from 5 M to 10 M), the treatment with higher concentrations of NaOH could bring more nanotubes into the sample as well as show higher catalytic activity. The higher proportion of nanotubes in the sample may be one reason for the higher catalytic activity. When the anatase was hydrothermally treated with 15 M NaOH, the sample exhibited the highest catalytic activity; however, the nanotubular structure of this sample was completely destroyed (Figure 3g–h). Similar observations can be obtained with respect to the rutile samples treated with different concentrations of NaOH (see Figure S2 in SM). Hence, we found that the nanotubular morphology is not mainly responsible for the high catalytic efficiency of the synthesized samples, which is consistent with previous work [7].

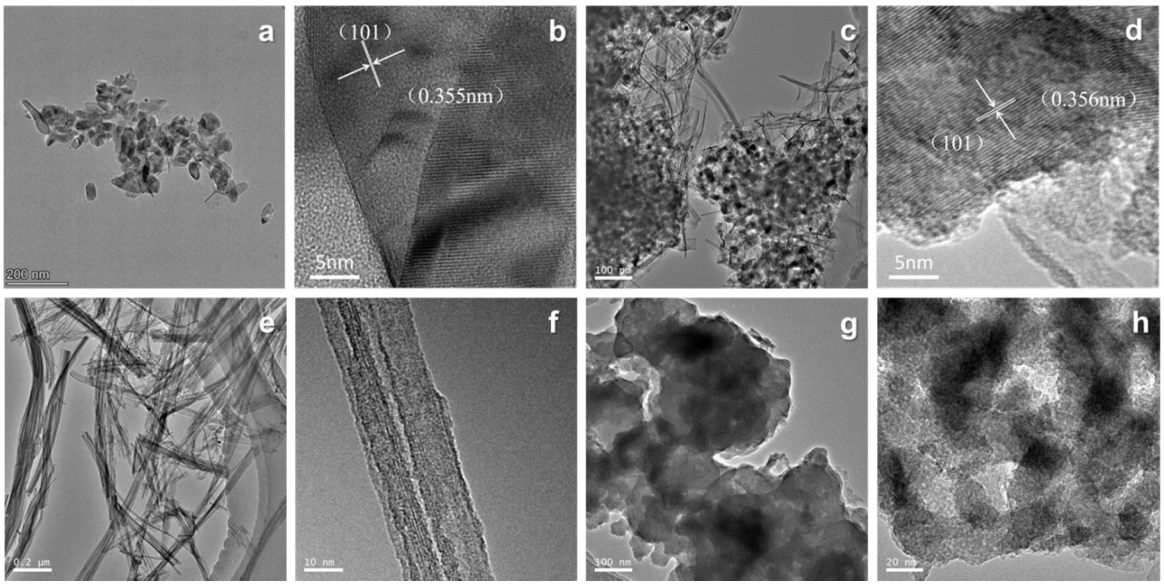

Figure 3. TEM images of catalysts originating from anatase TiO_2 with different concentrations of NaOH in hydrothermal processes: (**a**,**b**) for sample A-5, (**c**,**d**) for A-7.5, (**e**,**f**) for A-10, and (**g**,**h**) for A-15.

XRD analysis was further applied for the phase composition and crystal information of these catalysts, the results of which are exhibited in Figure 4. When comparing the XRD patterns of the synthesized catalysts with the original TiO_2 material (raw anatase or rutile), the samples that underwent NaOH hydrothermal treatment tended to change their crystal characteristic diffraction peaks: higher NaOH concentration would bring more change in XRD diffraction. Many works have stated that nanotubes originating from TiO_2 are actually titanate: sodium titanate and/or hydrogen titanate [26–29]. According to JCPDS card No. 47-0124, the catalysts A-10 or R-10 are mainly identified as $H_2Ti_2O_5 \cdot H_2O$, which is consistent with previous works [19,27,30]. In these two samples, the diffraction peak of anatase or rutile TiO_2 would be minimized. Hence, the anatase and rutile could be transformed into titanate as the NaOH concentration increased in the range of 0–10 M. In addition, the anatase samples that underwent NaOH hydrothermal treatment show less sharpness in their characteristic peaks and more amorphous structures, indicating lower crystallinity and smaller crystal size. The average crystal sizes and lattice spacings

of anatase D(101) or rutile D(110) of these samples were calculated based on the Scherrer formula and Bragg's Law [31–33] (see Table 1), while the anatase (101) peak of A-10 and A-15 as well as the rutile (110) peak of R-15 are absent in their XRD patterns, which is consistent with the data from TEM analysis. Nevertheless, the titanate diffraction peaks cannot be recognized in samples A-15 and R-15, most probably because they have been transformed into amorphous titanate due to the overdosed NaOH. Furthermore, materials originating from anatase or rutile TiO_2 show similar transformation trends when changing the NaOH concentration in the hydrothermal process.

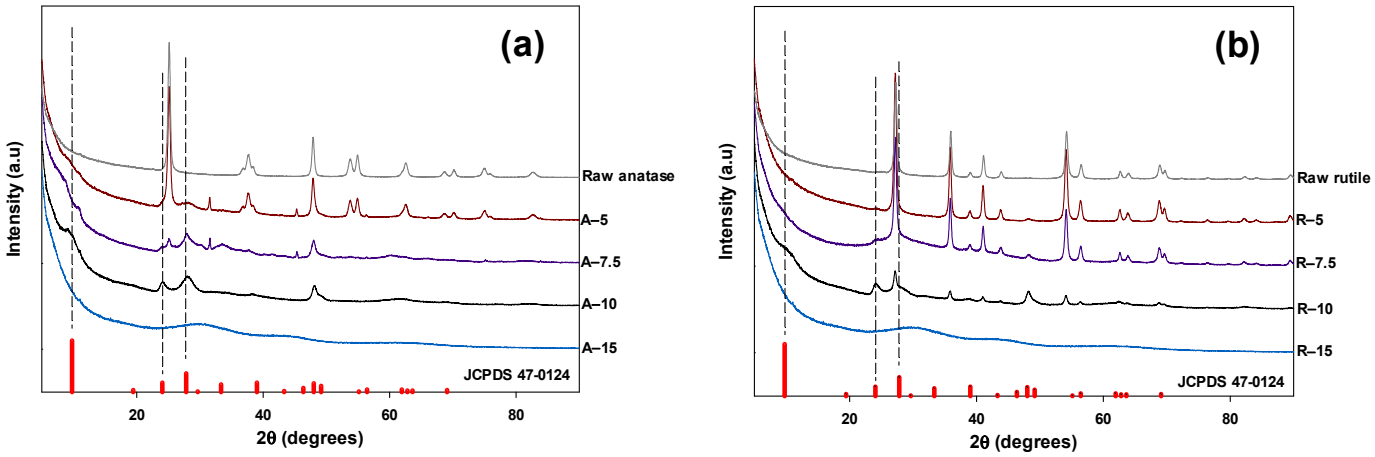

Figure 4. XRD patterns of the synthesized catalysts originating from anatase (**a**) and rutile (**b**) TiO_2 with different concentrations of NaOH in hydrothermal process.

Table 1. Characteristics of synthesized titania catalysts.

Sample ID	Crystal Size (nm)	D(101)/D(110) (Å) [1]	S_{BET} (m^2/g)
Raw anatase	22.7	3.54	66.95
A-5	21.2	3.54	75.83
A-7.5	21.6	3.54	108.6
A-10	NA	NA	219.3
A-15	NA	NA	16.26
Raw rutile	21.6	3.27	26.91
R-5	21.8	3.28	66.59
R-7.5	22	3.27	82.12
R-10	21.6	3.28	228.8
R-15	NA	NA	12.14

[1] D(101) for anatase materials and D(110) for rutile materials.

The BET surface area and pore size distribution of synthesized titania materials were measured (shown in Table 1, Figure 5 and Figure S3 in SM). Generally, the surface area of titania material, no matter whether originating from anatase or rutile, increased with increases in the applied concentration of NaOH in the hydrothermal process due to the formation of more nanotubes. TiO_2 samples treated with 10 M NaOH, A-10 and R-10, showed the highest BET surface areas of 219.3 m^2/g and 228.8 m^2/g, respectively. When overdosed NaOH was applied (i.e., 15 M), the surface area of the material reduced sharply because of the wrecked nanostructure. Hence, a higher specific surface area may not have a direct correlation with the higher catalytic efficiency of the synthesized catalysts. In addition, these titania materials show a relatively narrow distribution in pore size based on the Barrett–Joyner–Halebda (BJH) desorption data: around 3.6 nm and 8.0 nm for A-10, and around 3.4 nm and 22 nm for R-10. The pore sizes of 3.6 nm and 3.4 nm are inferred to be the internal diameters of the nanotubes, which agree well with the observations of TEM analysis.

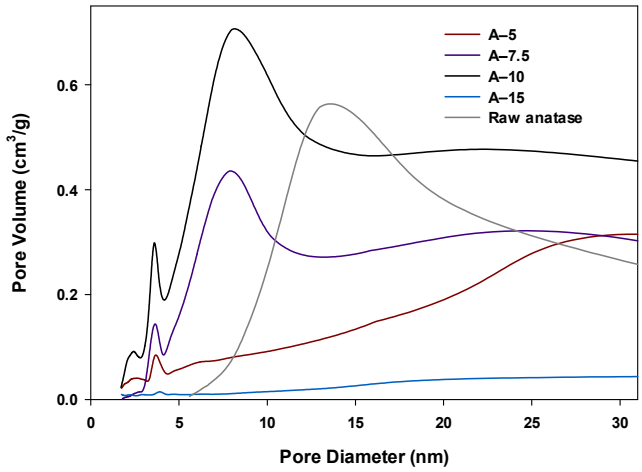

Figure 5. Pore size distribution of titania catalysts originating from anatase.

The materials were further characterized with Raman spectrometry, the results of which are exhibited in Figure 6. Five Raman bands at around 143, 197, 395, 515 and 638 cm^{-1} can be identified in the spectrum of the raw anatase TiO_2, which is consistent with the literature reports [31,34]. After hydrothermal treatment with NaOH (5 M–10 M), new Raman bands of 192, 275, 449, 667, 696, 835 and 920 cm^{-1} can be recognized, which correspond to the titanate nanotubes [26,30,35]. With respect to A-15, its Raman spectrum shows very notable features, containing several strong and sharp peaks at the lower frequency bands ranging from 80 to 310 cm^{-1}. According to the research work of Dr. Bamberger et al. [36], titanate ($Na_2Ti_6O_{13}$ or $H_2Ti_6O_{13}$) is considered to be the main species of this synthesized material. On the basis of the above observations, the sample prepared with a higher concentration of NaOH (5–15 M) formed more titanate ($Ti_2O_5^{2-}$ or $Ti_6O_{13}^{2-}$), which hints at a higher amount of titanate in the sample. This may be one reason for the higher catalytic efficiency of the synthesized samples.

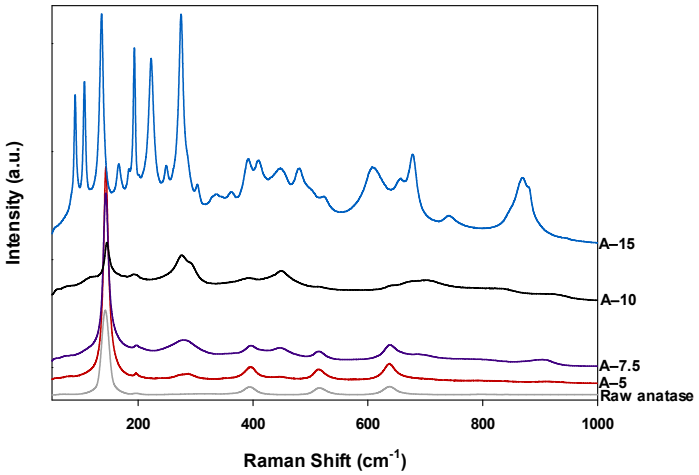

Figure 6. Raman spectra of titania catalysts originating from anatase TiO_2.

Many research works have argued that the surface OH groups of the catalysts play an important role in catalytic ozonation [7,37–39]. Hence, the densities of the surface hydroxyl groups of the synthesized materials were evaluated through FTIR analysis and a saturated (de)protonation approach according to the previous literature [7]. The vibration at around 1630 cm^{-1} in the FTIR spectra (Figure 7c,d) can be attributed to O-H bending vibration, while that at 3400 cm^{-1} corresponds to the OH stretching vibration [40]. Moreover, the intensity of vibrations increases with the concentration of NaOH used in hydrothermal treatment, indicating that a higher concentration of NaOH would bring more OH groups

onto the surface of the titania samples. The results of saturated (de)protonation also show that the density of surface OH groups of catalysts generally increases with the concentration of NaOH applied during the hydrothermal process (see Figure 7a,b). Among the synthesized catalysts, samples A-15 and R-15, which show the highest catalytic activities, have the highest density of surface OH groups of 1.43 mmol/g and 1.51 mmol/g, respectively. Furthermore, the catalytic rate constant is found to be nearly proportional to the density of surface hydroxyl groups of catalyst, so that a linear relation can be recognized, as shown in Figure 7a,b. Therefore, a high density of surface OH groups of catalyst should be essentially responsible for the high catalytic efficiency of the titania catalysts. Furthermore, the material originating from anatase shows a slightly higher density of surface OH groups compared with that from rutile, which hints at the role of raw materials.

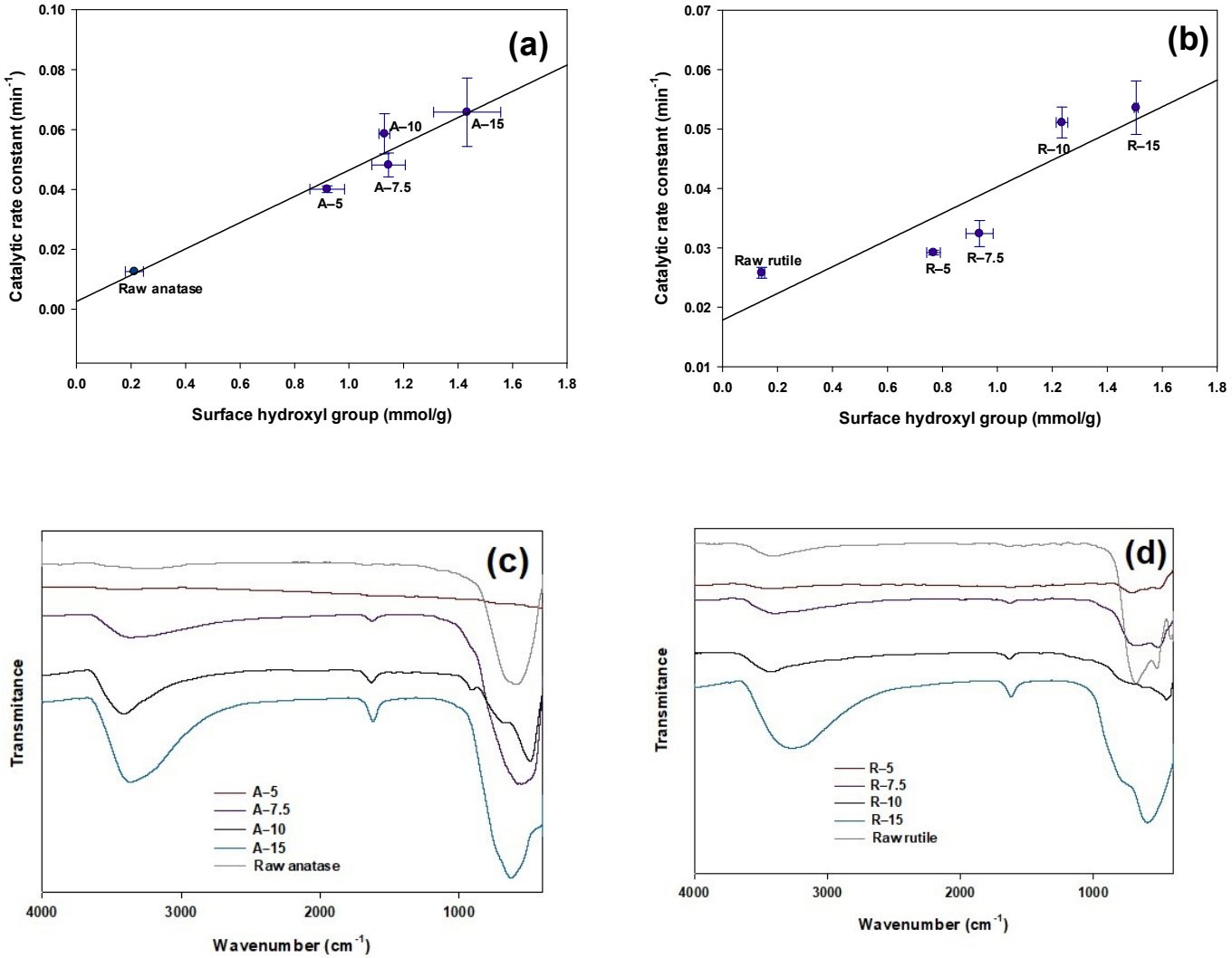

Figure 7. The linear relation between catalytic rate constant and density of surface hydroxyl groups of catalyst originating from anatase (**a**) and rutile (**b**) TiO_2; the FT-IR spectra of the catalyst originating from anatase (**c**) and rutile (**d**).

On the basis of the above discussion, a high density of surface OH groups of a catalyst, instead of nanotubular morphology or high surface area, should be the essential reason for the high catalytic activity of the synthesized titania catalysts. According to previous works, the synthesized titanate materials are rich in surface OH groups, especially in aqueous environments [41–44]. Hence, the synthesized materials with more titanate would have higher amount of hydroxyl groups, which would eventually result in higher catalytic

activity. Furthermore, the catalysts prepared from anatase show slightly higher activity than those from rutile, hinting at the minor impact of raw materials.

2.3. Active Oxidizing Species of Synthesized Titanate Catalysts

Many active oxidation species, such as hydroxyl radicals ($^{\bullet}OH$), singlet oxygen ($^1O_2$) and superoxide radicals ($^{\bullet}O_2^-$), can be detected in the catalytic ozonation process [45–47]. In this work, EPR spectroscopy was employed in order to determine the main active oxidizing species and their roles in the catalytic ozonation (see Figure 8 and Figure S4 in SM).

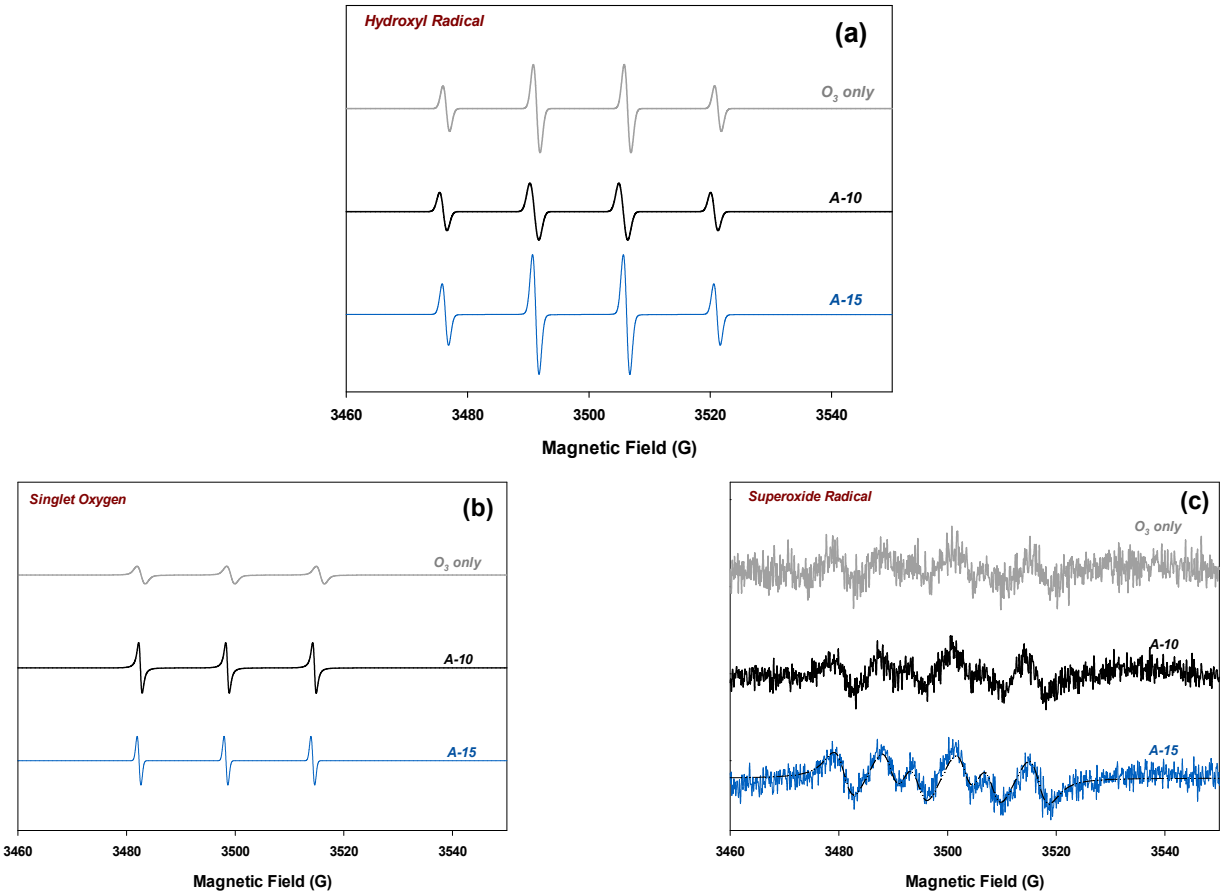

Figure 8. EPR spectra using (**a**) DMPO as hydroxyl radical trapping agent in water, (**b**) TEMP as singlet oxygen trapping agent in water, and (**c**) DMPO as superoxide radical trapping agent in absolute ethanol.

As shown in Figure 8a, clear characteristic peaks of DMPO-$^{\bullet}OH$ with hyperfine splitting constants of $\alpha_N = \alpha_H = 14.9$ G and a height ratio of quartet lines of 1:2:2:1 can be observed in all systems with or without catalysts, indicating the existence of $^{\bullet}OH$ during the catalytic ozonation or simple ozonation in this work. The peak intensity of the system with catalyst A-10 is slightly lower than that without the catalyst, suggesting $^{\bullet}OH$ is not mainly responsible for catalytic ozonation in this work. Although some research works have argued the significant importance of $^{\bullet}OH$ in catalytic ozonation [46–49], some others have confirmed the absence of $^{\bullet}OH$ in their processes [45,50]. The system with A-15 would have slightly higher intensity of DMPO-$^{\bullet}OH$ than others, hinting at the minor role of $^{\bullet}OH$ in this system, probably due to the amorphous state and the extremely high density of surface OH groups of A-15.

With respect to the role of singlet oxygen in catalytic ozonation in this work, the characteristic TEMP-$^1O_2$ peaks of triplet-line spectra with equal intensities can be observed in all systems, as exhibited in Figure 8b. Moreover, the intensities of the characteristic peak

of $^1O_2$ would be enhanced when synthesized titanate catalysts were applied in the system. Hence, $^1O_2$ is considered to be a dominant reactive oxidizing species that can accelerate formation in the catalytic process, which contributes to the higher catalytic efficiency of titanate catalysts. Similar phenomena are observed in Figure 8c of the DMPO-OOH EPR spectra, which suggests the synthesized catalysts can improve the generation of $^{\bullet}O_2^-$ in the system [51]. The EPR spectra of material originating from rutile (R-10) show very similar characteristics to those from anatase. Therefore, the singlet oxygen and superoxide radicals are the main active oxidation species of which more can be produced in the catalytic process, while the hydroxyl radical may only play a minor role (as shown in Scheme 1).

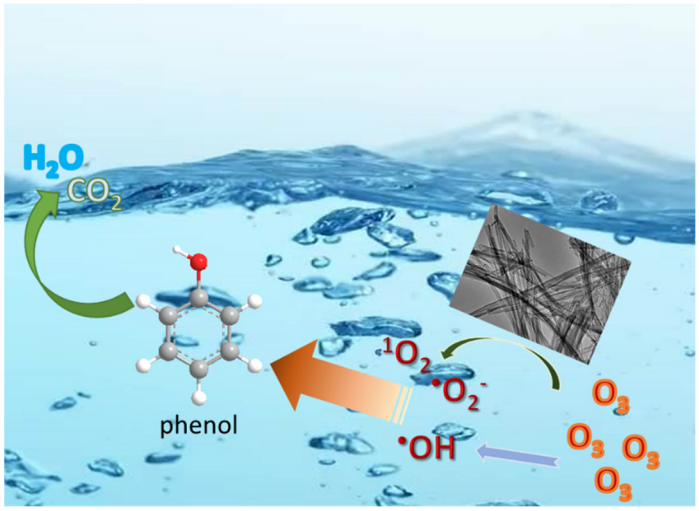

Scheme 1. Oxidizing mechanism of catalytic ozonation in this work.

3. Materials and Methods

3.1. Materials

The chemicals, including anatase titanium dioxide (99.8%, 25 nm), rutile titanium dioxide (99.8%, 25 nm), sodium hydroxide (NaOH, 96%), and phenol (99~100%) were purchased from Macklin Biochemical Co., Ltd. (Shanghai, China). Hydrochloric acid (HCl, 37%) was purchased from Lingfeng Chemical Reagent Co., Ltd. (Shanghai, China). Anhydrous ethanol (≥95%) was purchased from Anhui Ante Food Co., Ltd., while Acetonitrile (99.9%) was purchased from Aladdin Biochemical Technology Co., Ltd. (Shanghai, China). All chemicals were applied directly without further purification.

3.2. Synthesis of TiO_2 Nanomaterials

The synthesis of TiO_2 nanotubes was modified based on the hydrothermal approach reported previously [21]. The general procedure of synthesis is described below: 3 g of titanium dioxide (anatase or rutile) was dispersed in 75 mL of NaOH solution of different concentrations (5 M, 7.5 M, 10 M, and 15 M) in a Teflon-lined autoclave and thermally treated at 110 °C for 24 h. After cooling down, the obtained product was washed with 0.1 M HCl until the pH of supernatant was around 3, and washed with deionized water until the pH went to neutral. Finally, the solid product was dried with a freeze-dryer (LC-10N-50, Shanghai Lichen-BX Instrument Techonology Co., Ltd., Shanghai, China) to produce the as-synthesized TiO_2 nanomaterials. The synthesized samples originating from anatase were denoted as A-5, A-7.5, A-10, and A-15, while those originating from rutile were denoted as R-5, R-7.5, R-10, and R-15.

3.3. Experiments of Catalytic Ozonation

In order to investigate the catalytic activities of different TiO_2 nanotubes in ozonation, the experiments for the destruction of phenol (initial concentration: 20 mg/L) were conducted in a self-installed device, including an ozone generator (3S-T, Beijin Tonglin

Techonology Co., Ltd., Beijing, China), a mass flow controller (D07-19B, Beijin Sevenstar Flow Co., Ltd., Beijing, China), an ozone concentration analyzer (3S-J5000, Beijin Tonglin Techonology Co., Ltd., Beijing, China) and a glass reactor (120 mm (ø) × 150 mm (h)) with a thermal bath (22 ± 3 °C), as shown in Figure S5 in the Supplementary Material (SM). Generally, 1 g of catalyst was dispersed in 1 L of reaction solution in the reactor with continuous stirring; the O_3 and air mixture was introduced into the reactor at a flow rate of 50 mL/min; the concentration of O_3 was adjusted to be 10 mg/L; 3 mL liquid samples were taken after certain time intervals and filtered with PTFE syringe filters (0.45 μm). The residual O_3 in the off-gas was absorbed by KI solution.

The concentration of phenol in the obtained samples was quantified using a high-performance liquid chromatograph (HPLC, e2695, Waters, Milford, USA) with a 2489 UV/VIS detector set at 270 nm. An XBridge C_{18} column (250 mm × 4.6 mm, 5 μm particle size) was employed as the stationary phase, while a mixture of water and acetonitrile in a ratio of 50:50 (*v*:*v*) was applied as the mobile phase. The column temperature was set to be 30 °C, while the flow rate and injection volumes were 1 mL/min and 20 μL, respectively.

3.4. Characterization of TiO_2 Nanomaterials

The properties of the TiO_2 nanomaterials were characterized by several techniques. The XRD analysis was carried out on an Ultima IV multipurpose X-ray diffraction system (Rigaku, Tokyo, Japan) with Cu Kα radiation at 40 kV and 40 mA (λ = 1.5406 Å). JADE 6.5 software was applied for XRD spectra analysis. The Raman measurements were performed on a HORIBA JY LabRAM HR Evolution Raman spectrometer (HORIBA Scientific, Paris, France). The porosity as well as BET surface area of TiO_2 nanomaterials was investigated by applying a Micromeritics ASAP 2020 Surface Area and Porosity Analyzer (Micromeritics, Norcross, United States). The HR-TEM images were obtained using a FEI Talos F200S Transmission Electron Microscope (ThermoFisher, Waltham, USA) with a field emission-transmission gun at 200 kV, using a Digital Micrograph for image analysis. Fourier Transformed Infrared (FTIR) spectra in the transmission mode were measured with a Thermo Scientific Nicolet iS20 FTIR spectrometer (ThermoFisher, Waltham, USA) using KBr pellets. The electron paramagnetic resonance (EPR) experiments were carried out by employing EMXPlus in situ EPR spectrometer (Bruker, Karlsruhe, Germany) with DMPO or TEMP as trapping agents.

4. Conclusions

In the present work, titania catalysts synthesized with simple NaOH hydrothermal treatment without calcination were applied in ozonation for phenol removal. The catalysts treated with higher concentrations of NaOH contained more titanate, which facilitated more surface OH groups on the catalyst surface and eventually resulted in better catalytic activity. Furthermore, the main active oxidizing species of catalytic ozonation were recognized as singlet oxygen and superoxide radicals.

Supplementary Materials: The following supporting information can be downloaded at: https://www.mdpi.com/article/10.3390/molecules27092706/s1, Figure S1: $\ln(C_0/C)$ versus t when applying synthesized titania catalysts; Figure S2: TEM images of catalysts originating from rutile TiO_2 with different concentrations of NaOH in hydrothermal process: (a) and (b) for sample R-5, (c) and (d) for R-7.5, (e) and (f) for R-10, and (g) and (h) for R-15; Figure S3: Pore size distribution of titania catalysts originating from rutile; Figure S4: EPR spectra of catalyst R-10 using DMPO as hydroxyl radical trapping agent in water, TEMP as a singlet oxygen trapping agent in water, and DMPO as a superoxide radical trapping agent in absolute ethanol; Figure S5: Setup for experiments of catalytic ozonation.

Author Contributions: Conceptualization, G.Z. and Z.L.; methodology, G.Z.; software, A.J.; validation, L.L. and Z.L.; formal analysis, T.Y.; investigation, A.J.; resources, A.J.; data curation, A.J.; writing—original draft preparation, G.Z.; writing—review and editing, L.L.; visualization, H.W.; supervision, Z.L.; project administration, X.H.; funding acquisition, X.H. All authors have read and agreed to the published version of the manuscript.

Funding: This research was funded by Zhejiang Provincial Natural Science Foundation of China (grant number LQ19B070005) and Zhejiang Garden Pharmaceutical Corporation Limited (contract 2017330004001542 and project KYY-HX-20170062).

Institutional Review Board Statement: Not applicable.

Informed Consent Statement: Not applicable.

Data Availability Statement: All data is available in the main text or the Supplementary Materials.

Conflicts of Interest: The authors declare no conflict of interest.

Sample Availability: Samples of the compounds are available from the authors upon request.

References

1. Hiskia, A.; Dionysiou, D.D.; Antoniou, M.; Kaloudis, T. *Water Treatment for Purification from Cyanobacteria and Cyanotoxins*, 1st ed.; John Wiley & Sons: Hoboken, NJ, USA, 2020; p. 272.
2. Ledakowicz, S.; Pazdzior, K. Recent Achievements in Dyes Removal Focused on Advanced Oxidation Processes Integrated with Biological Methods. *Molecules* **2021**, *26*, 870. [CrossRef] [PubMed]
3. Imamovic, B.; Trebse, P.; Omeragic, E.; Becic, E.; Pecet, A.; Dedic, M. Stability and Removal of Benzophenone-Type UV Filters from Water Matrices by Advanced Oxidation Processes. *Molecules* **2022**, *27*, 1874. [CrossRef] [PubMed]
4. Liu, Y.; Zhang, Y.C.; Xu, X.F. Hydrothermal synthesis and photocatalytic activity of CdO_2 nanocrystals. *J. Hazard. Mater.* **2009**, *163*, 1310–1314. [CrossRef] [PubMed]
5. Hu, E.L.; Shang, S.M.; Chiu, K.L. Removal of Reactive Dyes in Textile Effluents by Catalytic Ozonation Pursuing on-Site Effluent Recycling. *Molecules* **2019**, *24*, 2755. [CrossRef]
6. Inchaurrondo, N.S.; Font, J. Clay, Zeolite and Oxide Minerals: Natural Catalytic Materials for the Ozonation of Organic Pollutants. *Molecules* **2022**, *27*, 2151. [CrossRef]
7. Song, S.; Liu, Z.W.; He, Z.Q.; Zhang, A.L.; Chen, J.M. Impacts of Morphology and Crystallite Phases of Titanium Oxide on the Catalytic Ozonation of Phenol. *Environ. Sci. Technol.* **2010**, *44*, 3913–3918. [CrossRef]
8. Yang, Y.X.; Ma, J.; Qin, Q.D.; Zhai, X.D. Degradation of nitrobenzene by nano-TiO_2 catalyzed ozonation. *J. Mol. Catal. A-Chem.* **2007**, *267*, 41–48. [CrossRef]
9. Yang, Y.X.; Ma, J.; Zhang, J.; Wang, S.J.; Qin, Q.D. Ozonation of Trace Nitrobenzene in Water in the Presence of a TiO2/Silica-Gel Catalyst. *Ozone-Sci. Eng.* **2009**, *31*, 45–52. [CrossRef]
10. Wang, S.J.; Ma, J.; Yang, Y.X.; Zhang, J.; Liang, T. Degradation and Transformation of Organic Compounds in Songhua River Water by Catalytic Ozonation in the Presence of TiO(2)/Zeolite. *Ozone-Sci. Eng.* **2011**, *33*, 236–242. [CrossRef]
11. Anandan, S.; Wu, J.J. Effective Degradation of Fipronil Using Combined Catalytic Ozonation Processes. *Ozone-Sci. Eng.* **2015**, *37*, 186–190. [CrossRef]
12. Rosal, R.; Gonzalo, M.S.; Boltes, K.; Leton, P.; Vaquero, J.J.; Garcia-Calvo, E. Identification of intermediates and assessment of ecotoxicity in the oxidation products generated during the ozonation of clofibric acid. *J. Hazard. Mater.* **2009**, *172*, 1061–1068. [CrossRef] [PubMed]
13. Keri, O.; Kocsis, E.; Karajz, D.A.; Nagy, Z.K.; Parditka, B.; Erdelyi, Z.; Szabo, A.; Hernadi, K.; Szilagyi, I.M. Photocatalytic Crystalline and Amorphous TiO_2 Nanotubes Prepared by Electrospinning and Atomic Layer Deposition. *Molecules* **2021**, *26*, 5917. [CrossRef] [PubMed]
14. Appadurai, T.; Subramaniyam, C.M.; Kuppusamy, R.; Karazhanov, S.; Subramanian, B. Electrochemical Performance of Nitrogen-Doped TiO_2 Nanotubes as Electrode Material for Supercapacitor and Li-Ion Battery. *Molecules* **2019**, *24*, 2952. [CrossRef] [PubMed]
15. Udrescu, A.; Florica, S.; Chivu, M.; Mercioniu, I.; Matei, E.; Baibarac, M. Rhodamine B Photodegradation in Aqueous Solutions Containing Nitrogen Doped TiO_2 and Carbon Nanotubes Composites. *Molecules* **2021**, *26*, 7237. [CrossRef] [PubMed]
16. Kitano, M.; Wada, E.; Nakajima, K.; Hayashi, S.; Miyazaki, S.; Kobayashi, H.; Hara, M. Protonated Titanate Nanotubes with Lewis and Bronsted Acidity: Relationship between Nanotube Structure and Catalytic Activity. *Chem. Mater.* **2013**, *25*, 385–393. [CrossRef]
17. Sandoval, A.; Hernandez-Ventura, C.; Klimova, T.E. Titanate nanotubes for removal of methylene blue dye by combined adsorption and photocatalysis. *Fuel* **2017**, *198*, 22–30. [CrossRef]
18. Yu, J.G.; Yu, H.G.; Cheng, B.; Trapalis, C. Effects of calcination temperature on the microstructures and photocatalytic activity of titanate nanotubes. *J. Mol. Catal. A-Chem.* **2006**, *249*, 135–142. [CrossRef]
19. Liu, Z.W.; Qiu, J.P.; Zheng, C.C.; Li, L.Q. Degradation of the Ammonia Wastewater in Aqueous Medium with Ozone in Combination with Mesoporous TiO_2 Catalytic. *AIP Conf. Proc.* **2017**, *1820*.
20. Xing, S.T.; Lu, X.Y.; Zhang, X.J.; Zhang, Y.Y.; Ma, Z.C.; Wu, Y.S. Mechanism for catalytic ozonation of p-nitrophenol in water with titanate nanotube supported manganese oxide. *RSC Adv.* **2015**, *5*, 101975–101981. [CrossRef]
21. Tsai, C.C.; Teng, H.S. Regulation of the physical characteristics of Titania nanotube aggregates synthesized from hydrothermal treatment. *Chem. Mater.* **2004**, *16*, 4352–4358. [CrossRef]

22. Molnar, J.; Agbaba, J.; Dalmacija, B.; Klasnja, M.; Watson, M.; Kragulj, M. Effects of Ozonation and Catalytic Ozonation on the Removal of Natural Organic Matter from Groundwater. *J. Environ. Eng.* **2012**, *138*, 804–808. [CrossRef]
23. Lanao, M.; Ormad, M.P.; Ibarz, C.; Miguel, N.; Ovelleiro, J.L. Bactericidal Effectiveness of O_3, O_3/H_2O_2 and O_3/TiO_2 on Clostridium perfringens. *Ozone-Sci. Eng.* **2008**, *30*, 431–438. [CrossRef]
24. Ormad, M.P.; Miguel, N.; Lanao, M.; Mosteo, R.; Ovelleiro, J.L. Effect of Application of Ozone and Ozone Combined with Hydrogen Peroxide and Titanium Dioxide in the Removal of Pesticides From Water. *Ozone-Sci. Eng.* **2010**, *32*, 25–32. [CrossRef]
25. Chen, Y.H.; Hsieh, D.C.; Shang, N.C. Efficient mineralization of dimethyl phthalate by catalytic ozonation using TiO_2/Al_2O_3 catalyst. *J. Hazard. Mater.* **2011**, *192*, 1017–1025. [CrossRef] [PubMed]
26. Maxim, F.; Ferreira, P.; Vilarinho, P.M. Influence of the neutralization process on the preparation of titanate nanotubes by hydrothermal synthesis. *J. Porous Mat.* **2011**, *18*, 37–45. [CrossRef]
27. Tsai, C.C.; Teng, H.S. Structural features of nanotubes synthesized from NaOH treatment on TiO_2 with different post-treatments. *Chem. Mater.* **2006**, *18*, 367–373. [CrossRef]
28. Lu, D.Z.; Yang, M.C.; Kumar, K.K.; Wu, P.; Neena, D. Investigation of Structure and Photocatalytic Degradation of Organic Pollutants for Protonated Anatase/Titanate Nanosheets during Thermal Treatment. *Acs Sustain. Chem. Eng.* **2018**, *6*, 4801–4808. [CrossRef]
29. Uematsu, E.; Itadani, A.; Hashimoto, H.; Uematsu, K.; Toda, K.; Sato, M. Tubular Titanates: Alkali-Metal Ion-Exchange Features and Carbon Dioxide Adsorption at Room Temperature. *Ind. Eng. Chem. Res.* **2019**, *58*, 5168–5174. [CrossRef]
30. Gao, T.; Fjellvag, H.; Norby, P. Crystal Structures of Titanate Nanotubes: A Raman Scattering Study. *Inorg. Chem.* **2009**, *48*, 1423–1432. [CrossRef]
31. Huang, X.W.; Yang, W.Q.; Zhang, G.S.; Yan, L.; Zhang, Y.C.; Jiang, A.H.; Xu, H.L.; Zhou, M.; Liu, Z.J.; Tang, H.D.; et al. Alternative synthesis of nitrogen and carbon co-doped TiO_2 for removing fluoroquinolone antibiotics in water under visible light. *Catal. Today* **2021**, *361*, 11–16. [CrossRef]
32. Ge, T.; Jiang, Z.; Shen, L.; Li, J.; Lu, Z.; Zhang, Y.; Wang, F. Synthesis and application of $Fe_3O_4/FeWO_4$ composite as an efficient and magnetically recoverable visible light-driven photocatalyst for the reduction of Cr(VI). *Sep. Purif. Technol.* **2021**, *263*, 118401. [CrossRef]
33. Jaramillo-Fierro, X.; González, S.; Medina, F. La-Doped $ZnTiO_3/TiO_2$ Nanocomposite Supported on Ecuadorian Diatomaceous Earth as a Highly Efficient Photocatalyst Driven by Solar Light. *Molecules* **2021**, *26*, 6232. [CrossRef] [PubMed]
34. Giarola, M.; Sanson, A.; Monti, F.; Mariotto, G.; Bettinelli, M.; Speghini, A.; Salviulo, G. Vibrational dynamics of anatase TiO_2: Polarized Raman spectroscopy and ab initio calculations. *Phys. Rev. B* **2010**, *81*, 174305. [CrossRef]
35. Ma, R.Z.; Fukuda, K.; Sasaki, T.; Osada, M.; Bando, Y. Structural features of titanate nanotubes/nanobelts revealed by Raman, X-ray absorption fine structure and electron diffraction characterizations. *J. Phys. Chem. B* **2005**, *109*, 6210–6214. [CrossRef]
36. Bamberger, C.E.; Begun, G.M. Sodium Titanates: Stoichiometry and Raman Spectra. *J. Am. Ceram. Soc.* **1987**, *70*, C-48–C-51. [CrossRef]
37. Ma, W.F.; Hu, J.Z.; Yoza, B.A.; Wang, Q.H.; Zhang, X.F.; Li, Q.X.; Guo, S.H.; Chen, C.M. Kaolinite based catalysts for efficient ozonation of recalcitrant organic chemicals in water. *Appl. Clay Sci.* **2019**, *175*, 159–168. [CrossRef]
38. Yuan, L.; Shen, J.M.; Chen, Z.L.; Guan, X.H. Role of Fe/pumice composition and structure in promoting ozonation reactions. *Appl. Catal. B-Environ.* **2016**, *180*, 707–714. [CrossRef]
39. Zhao, L.; Ma, W.C.; Lu, S.; Ma, J. Influencing investigation of metal ions on heterogeneous catalytic ozonation by ceramic honeycomb for the degradation of nitrobenzene in aqueous solution with neutral pH. *Sep. Purif. Technol.* **2019**, *210*, 167–174. [CrossRef]
40. Reda, S.M.; Khairy, M.; Mousa, M.A. Photocatalytic activity of nitrogen and copper doped TiO_2 nanoparticles prepared by microwave-assisted sol-gel process. *Arab. J. Chem.* **2020**, *13*, 86–95. [CrossRef]
41. Takadama, H.; Kim, H.M.; Kokubo, T.; Nakamura, T. An X-ray photoelectron spectroscopy study of the process of apatite formation on bioactive titanium metal. *J. Biomed Mater. Res.* **2001**, *55*, 185–193. [CrossRef]
42. Wang, L.M.; Zhou, B.B.; Huang, X.X.; Dong, L.Q.; Cheng, K.; Weng, W.J. Cell responses on a $H_2Ti_3O_7$ nanowire film. *RSC Adv.* **2017**, *7*, 33606–33613. [CrossRef]
43. Hernandez-Alonso, M.D.; Garcia-Rodriguez, S.; Suarez, S.; Portela, R.; Sanchez, B.; Coronado, J.M. Operando DRIFTS study of the role of hydroxyls groups in trichloroethylene photo-oxidation over titanate and TiO_2 nanostructures. *Catal. Today* **2013**, *206*, 32–39. [CrossRef]
44. Jiang, J.; Gao, Q.; Chen, Z. Gold nanocatalysts supported on protonic titanate nanotubes and titania nanocrystals. *J. Mol. Catal. A-Chem.* **2008**, *280*, 233–239. [CrossRef]
45. Wang, Y.X.; Xie, Y.B.; Sun, H.Q.; Xiao, J.D.; Cao, H.B.; Wang, S.B. Hierarchical shape-controlled mixed-valence calcium manganites for catalytic ozonation of aqueous phenolic compounds. *Catal. Sci. Technol.* **2016**, *6*, 2918–2929. [CrossRef]
46. Wang, D.; Xu, H.D.; Ma, J.; Lu, X.H.; Qi, J.Y.; Song, S. Morphology Control Studies of $MnTiO_3$ Nanostructures with Exposed {0001} Facets as a High-Performance Catalyst for Water Purification. *ACS Appl. Mater. Int.* **2018**, *10*, 31631–31640. [CrossRef]
47. Guo, Y.; Zhang, Y.X.; Yu, G.; Wang, Y.J. Revisiting the role of reactive oxygen species for pollutant abatement during catalytic ozonation: The probe approach versus the scavenger approach. *Appl. Catal. B-Environ.* **2021**, *280*, 119418. [CrossRef]

48. Song, Z.L.; Wang, M.X.; Wang, Z.; Wang, Y.F.; Li, R.Y.; Zhang, Y.T.; Liu, C.; Liu, Y.; Xu, B.B.; Qi, F. Insights into Heteroatom-Doped Graphene for Catalytic Ozonation: Active Centers, Reactive Oxygen Species Evolution, and Catalytic Mechanism. *Environ. Sci. Technol.* **2019**, *53*, 5337–5348. [CrossRef]
49. Afzal, S.; Quan, X.; Zhang, J.L. High surface area mesoporous nanocast $LaMO_3$ (M = Mn, Fe) perovskites for efficient catalytic ozonation and an insight into probable catalytic mechanism. *Appl. Catal. B-Environ.* **2017**, *206*, 692–703. [CrossRef]
50. Wang, Y.X.; Xie, Y.B.; Sun, H.Q.; Xiao, J.D.; Cao, H.B.; Wang, S.B. Efficient Catalytic Ozonation over Reduced Graphene Oxide for p-Hydroxylbenzoic Acid (PHBA) Destruction: Active Site and Mechanism. *Acs Appl. Mater. Int.* **2016**, *8*, 9710–9720. [CrossRef]
51. Han, R.R.; Fang, Y.S.; Sun, P.; Xie, K.; Zhai, Z.C.; Liu, H.X.; Liu, H. N-Doped Biochar as a New Metal-Free Activator of Peroxymonosulfate for Singlet Oxygen-Dominated Catalytic Degradation of Acid Orange 7. *Nanomaterials* **2021**, *11*, 2288. [CrossRef]